nature neuroscience

Zeb2 is essential for Schwann cell differentiation, myelination and nerve repair

Susanne Quintes[1,2,9], Bastian G Brinkmann[1,9], Madlen Ebert[1], Franziska Fröb[3], Theresa Kungl[1], Friederike A Arlt[1], Victor Tarabykin[4], Danny Huylebroeck[5,6], Dies Meijer[7], Ueli Suter[8], Michael Wegner[3], Michael W Sereda[1,2,10] & Klaus-Armin Nave[1,10]

Schwann cell development and peripheral nerve myelination require the serial expression of transcriptional activators, such as Sox10, Oct6 (also called Scip or Pou3f1) and Krox20 (also called Egr2). Here we show that transcriptional repression, mediated by the zinc-finger protein Zeb2 (also known as Sip1), is essential for differentiation and myelination. Mice lacking *Zeb2* in Schwann cells develop a severe peripheral neuropathy, caused by failure of axonal sorting and virtual absence of myelin membranes. *Zeb2*-deficient Schwann cells continuously express repressors of lineage progression. Moreover, genes for negative regulators of maturation such as Sox2 and Ednrb emerge as Zeb2 target genes, supporting its function as an 'inhibitor of inhibitors' in myelination control. When *Zeb2* is deleted in adult mice, Schwann cells readily dedifferentiate following peripheral nerve injury and become repair cells. However, nerve regeneration and remyelination are both perturbed, demonstrating that Zeb2, although undetectable in adult Schwann cells, has a latent function throughout life.

The successive developmental stages of Schwann cell proliferation, axon sorting and myelination are regulated by a feed-forward cascade of transcriptional activators that ultimately upregulate a large number of genes encoding myelination-associated enzymes and myelin structural proteins[1–3]. Well-studied examples include the transcription factor Krox20, as illustrated by *Krox20* mutant Schwann cells, which successfully sort axons but fail to generate or maintain myelin membranes[4,5], and the transcription factors Oct6 and Sox10, which are developmentally upstream of and directly interact with Krox20 to promote Schwann cell differentiation and myelination[6,7]. Studies on constitutive and conditional *Sox10* mutant mice reveal an essential role of this transcription factor in Schwann cell specification, lineage progression, differentiation, myelin formation and maintenance[8–11].

Most research on the genetic control of Schwann cell differentiation has concentrated on transcriptional activators that would generate positive feed-forward loops when uncontrolled. This raises the question how Schwann cell differentiation is properly balanced. Transcriptional repressors are plausible candidates. For example, the co-repressor Nab (also called NGFI-A–binding or Egr-binding protein) is essential for peripheral nervous system (PNS) myelination[12]. However, when associated with Krox20 this protein is a coactivator of myelin protein genes, and the significance of gene repression by Nab–Krox20 complexes in Schwann cells is unclear[13,14]. The zinc-finger protein Yin-Yang 1 (Yy1), an essential transcriptional inhibitor in myelinating oligodendrocytes[15], has so far only been characterized as a transcriptional activator in the PNS, immediately upstream of Krox20 (ref. 16). Other transcription factors have been functionally identified as 'negative regulators' of myelination, but these include both transcriptional activators (for example, Sox2, c-Jun, Pax3, Notch-ICD) and inhibitors (Id2). While the most likely function of these factors is driving Schwann cell dedifferentiation after injury and in preparation for nerve repair[1], their presence interferes with myelination and myelin maintenance.

Zinc-finger E-box-binding homeobox 2 (Zeb2, also known as Sip1 or Zfhx1b) is a widely expressed zinc-finger homeobox protein, originally identified by its binding to Smad1 (refs. 17,18). During epithelial-to-mesenchymal transition, Zeb2 represses the transcription of several genes for cell adhesion molecules, such as E-cadherin (refs. 19–21). In the CNS, newly born neurons express Zeb2 to downregulate signaling proteins that drive neurogenesis of adjacent precursors[22]. Zeb2 also regulates oligodendrocyte differentiation, as mutant cells fail to fully mature and make myelin[23].

Like Sox10, Zeb2 is also detectable early in the neural crest lineage[24] and therefore a plausible candidate for transcriptional regulation in the Schwann cell lineage. In humans, mutations of *SOX10* and *ZEB2* have been associated with the clinically related Waardenburg syndrome type 4 and Mowat-Wilson syndrome, respectively[25]. For neural crest cells, direct interactions of Sox10 and Zeb2 proteins have even been proposed, but this is again difficult to reconcile with their respective roles as transcriptional activators and repressors[26]. Zeb2

[1]Department of Neurogenetics, Max Planck Institute of Experimental Medicine, Göttingen, Germany. [2]Department of Clinical Neurophysiology, University Medical Center Göttingen (UMG), Göttingen, Germany. [3]Institut für Biochemie, Emil-Fischer-Zentrum, Friedrich-Alexander Universität Erlangen-Nürnberg, Erlangen, Germany. [4]Institute for Cell and Neurobiology, Center for Anatomy, Charité Universitätsmedizin Berlin, Berlin, Germany. [5]Department of Development and Regeneration, Laboratory of Molecular Biology (Celgen), KU Leuven, Leuven, Belgium. [6]Department of Cell Biology, Erasmus University Medical Center, Rotterdam, the Netherlands. [7]Centre for Neuroregeneration, University of Edinburgh, Edinburgh, UK. [8]Department of Biology, Institute of Molecular Health Sciences, ETH Zürich, Zürich, Switzerland. [9]These authors contributed equally to this work. [10]These authors jointly directed this work. Correspondence should be addressed to M.W.S. (sereda@em.mpg.de) or K.-A.N. (nave@em.mpg.de).

Received 22 February; accepted 4 May; published online 13 June 2016; doi:10.1038/nn.4321

is a canonical transcriptional repressor and, in neural-crest-derived immature Schwann cells, a candidate to 'release the brake' on differentiation that might be imposed by negative regulators, such as Sox2.

Here, we show that Zeb2 targets are indeed inhibitors of Schwann cell differentiation. Mice lacking *Zeb2* specifically in this lineage show a complete arrest of Schwann cell maturation and exhibit a virtually complete absence of myelin. However, *Zeb2*-deficient Schwann cells survive *in vivo* and maintain axonal integrity. While Zeb2 is not required for adult myelin maintenance and axonal integrity, after injury *Zeb2*-deficient Schwann cells fail to efficiently support nerve regeneration.

RESULTS

Zeb2 is expressed in Schwann cell development and after injury

To explore Zeb2 expression by Schwann cells, we immunostained paraffin sections of mouse sciatic nerves at different developmental stages. Zeb2 was exclusively localized to cell nuclei. At embryonic day (E) 18.5, about 90% of Schwann cells were Zeb2-positive. At postnatal day (P) 10, roughly 70% of cells were Zeb2-positive, and in adult mice virtually all Schwann cells were Zeb2-negative (**Fig. 1a**).

To study the Schwann cell-specific function of Zeb2, we bred mice containing a *loxP*-flanked *Zeb2* allele[27] to mice expressing Cre under control of the Desert hedgehog promoter, leading to recombination in the Schwann cell lineage between E11 and E13.5 (refs. 9,28), when most cells are at the precursor stage[29]. Loss of Zeb2 protein was confirmed by the absence of immunostaining (**Fig. 1a**) and by analysis of steady-state mRNA levels in sciatic nerve at age P1 (reduction to 14.1% of control; data not shown).

To determine possible Zeb2 re-expression in Schwann cells after acute sciatic nerve injury, we stained paraffin sections of the distal segment at different time points after a nerve crush (**Fig. 1b**). Zeb2 was detected as early as 6 h after injury (data not shown), and 80% of all cells could be stained 7 d after injury (**Fig. 1b**). On day 14 after crush, when remyelination is at its peak, about 50% of all Schwann cells still expressed Zeb2 (**Fig. 1b**). Zeb2 was absent from distal stumps 28 d after crush (**Fig. 1b**), and we could not detect Zeb2-positive cells in the contralateral uninjured nerve (**Fig. 1b**). We conclude that Zeb2 expression is transient in peripheral nerves, preceding myelination in development and remyelination after acute nerve injury.

Zeb2 in Schwann cells is essential for axon sorting and myelination

Conditional mutants (*Dhh-cre::Zeb2*$^{loxP/loxP}$) were born at the expected Mendelian ratio and phenotypically distinguishable from littermate controls by the second postnatal week, when they had reduced body size and developed ataxia and hind limb weakness (**Supplementary Video 1**). The latter progressed with age but never led to complete hind limb paralysis. It was unexpectedly difficult to record compound muscle action potentials (CMAP) when electrically stimulating the sciatic nerve of conditional mutants compared

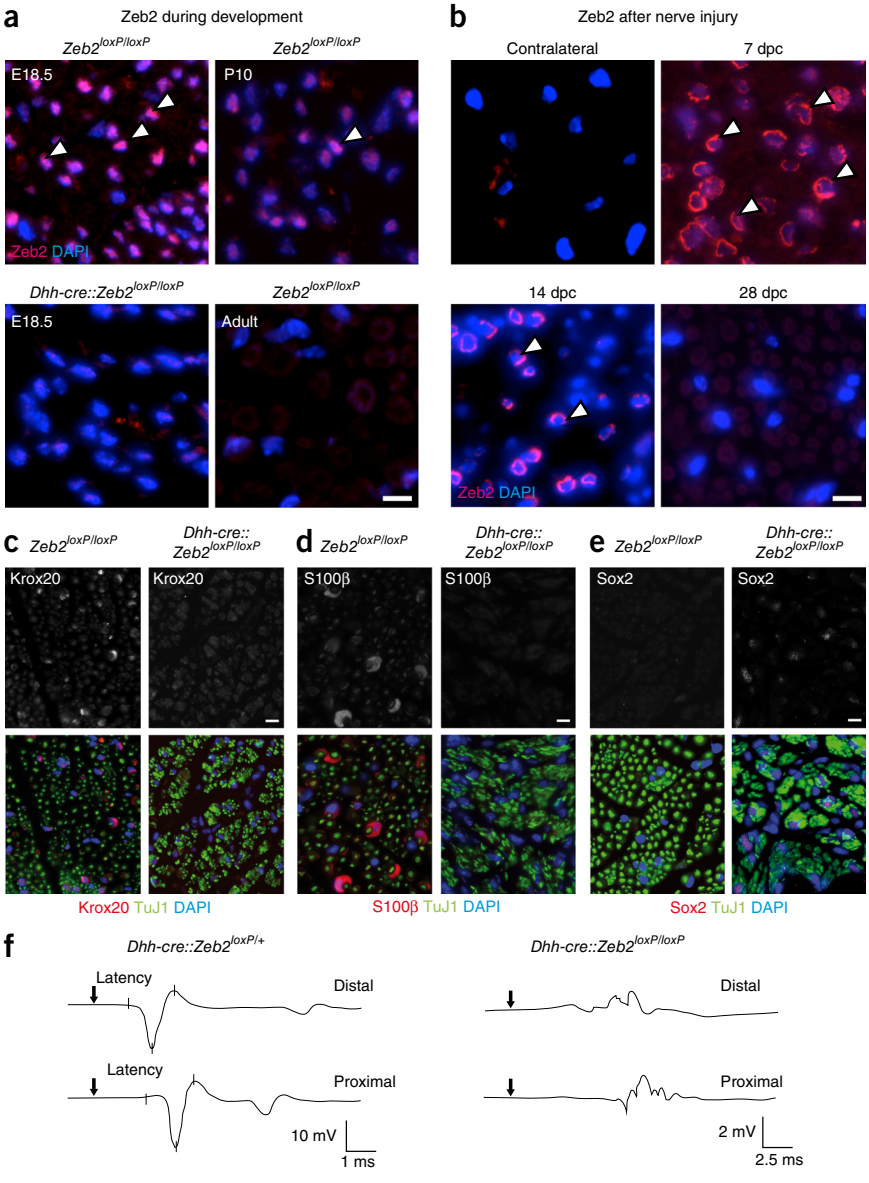

Figure 1 Functional analysis of Zeb2 in Schwann cell development and nerve repair. (**a**) Nuclear Zeb2 immunofluorescence (pink, white arrowheads) of sciatic nerve cross-sections at different developmental stages. Zeb2 is absent from Schwann cells of *Dhh-cre::Zeb2*$^{loxP/loxP}$ mice at E18.5 (lower left). Representative images of $n = 3$ animals per time point and genotype. Scale bar, 10 µm. (**b**) Zeb2 re-expression at different time points after nerve crush in the distal stump of sciatic nerves (pink, white arrowheads; dpc, days post crush; contralateral, unharmed nerve). Representative images of $n = 3$ animals per time point and genotype. Scale bar, 10 µm. (**c**–**e**) Immunohistochemistry of sciatic nerve cross-sections from *Dhh-cre::Zeb2*$^{loxP/loxP}$ mice and controls at P25 comparing Krox20 (**c**), S100β (**d**) and Sox2 (**e**). Axons, green (TuJ1); Schwann cell nuclei, blue (DAPI). Representative images of $n = 3$ animals per genotype. Scale bars, 10 µm. Experiments in panels **a**–**e** were successfully repeated in 3 animals per genotype and time point. (**f**) Electrophysiological recording of CMAPs with proximally and distally stimulated sciatic nerves from *Dhh-cre::Zeb2*$^{loxP/+}$ mice (left) and *Dhh-cre::Zeb2*$^{loxP/loxP}$ mice (right) at age P25. Representative traces from measurements of 3 mice per genotype are shown.

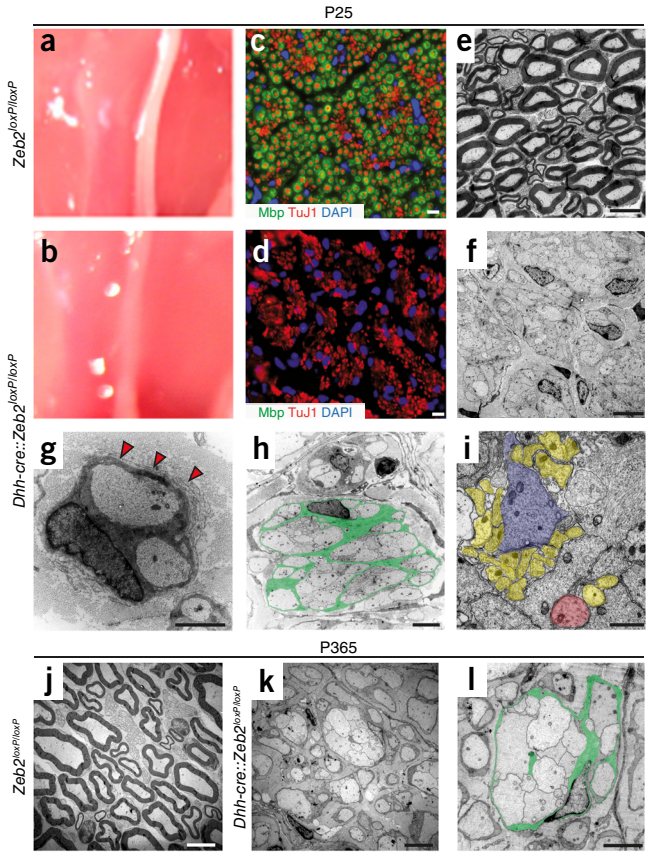

Figure 2 Mice lacking Zeb2 in Schwann cells develop severe neuropathy. (**a**,**b**) Compared to control sciatic nerves at age P25, *Dhh-cre::Zeb2*$^{loxP/loxP}$ mutant nerves are translucent. (**c**,**d**) Mbp-stained myelin (green) surrounds TuJ1 stained axons (red). Note the absence of myelin in **d**. DAPI, Schwann cell nuclei. Scale bars, 10 µm. The experiment was successfully repeated in 3 animals per genotype and representative images are shown. (**e**,**f**) Electron microscopy of control nerves (**e**) and mutant nerves (**f**) shows that mutant nerves are amyelinated. Scale bars, 2.5 µm. (**g**) *Zeb2*-deficient Schwann cell arrested in sorting with two engulfed axons and supernumerary loops of basal lamina (red arrowheads). Scale bar, 1 µm. (**h**) Mutant Schwann cell (cytoplasm, green) surrounding >50 axons without sorting. Scale bar, 1 µm. (**i**) Bundle of unsorted axons that differ in size, as indicated by false colors (yellow, small; red, medium; purple, large). Scale bar, 1 µm. (**j**–**l**) At 1 year of age, conditional mutants showed persistent lack of sorting and amyelination (**k**,**l**) compared to control (**j**). Green, Schwann cell cytoplasm. Axons appear intact. Scale bars, 2.5 µm. All electron micrographs shown in panels **e**–**l** are representative of 3 mice per genotype and age.

to heterozygous controls (**Fig. 1f**), which suggests major conduction blocks. However, *Zeb2* conditional mutants had a normal life span and we only occasionally observed unexplained premature deaths.

To assess the developmental stage of *Zeb2*-deficient Schwann cells, we immunostained cross-sections from mutants and controls for Krox20 and Sox2 as prototype positive and negative regulators, respectively. We used S100β as a marker for both immature and mature Schwann cells. While Schwann cells in control mice robustly expressed Krox20 and S100β and were negative for Sox2, only a few *Zeb2*-deficient Schwann cells expressed Krox20 and S100β but about 30% were positive for Sox2 (**Fig. 1c**–**e**).

At P25, the sciatic nerves of mutant mice were thinner and more translucent than those of controls (**Fig. 2a**,**b**). Immunostaining of cross-sections for axonal β-tubulin (TuJ1) and myelin basic protein (Mbp) revealed closely packed, amyelinated axons in mutants but not in controls (**Fig. 2c**,**d**). Electron microscopy revealed that *Zeb2*-deficient mice lacked peripheral myelination and showed abnormal axon bundles, with Schwann cells engulfing larger groups of axons that also greatly varied in diameter (**Fig. 2e**–**i**). Within these bundles, interdigitating Schwann cell processes could be observed, but the majority of axons remained closely packed, resembling axons associated with immature Schwann cells in embryonic nerves (**Fig. 2i**). Most Schwann cells failed to establish one-to-one relationships with axons. We noticed that the basal lamina of *Zeb2*-deficient Schwann cells was often thin, discontinuous and not attached to the glial cell membrane, providing a plausible cause of failed axonal sorting[30]. Many Schwann cells also displayed redundant basal lamina loops (**Fig. 2g**).

At 1 year of age, peripheral axons had grown in diameter, but the overall pathology appeared unchanged (**Fig. 2j**–**l**). Compared to P25, the total Schwann cell number was unaltered in mutants (**Supplementary Fig. 1a**). Accordingly, the percentage of bromodeoxyuridine (BrdU)-positive (proliferating) cells did not differ between mutants and controls at E18.5, P10 and P25 (**Supplementary Fig. 1b**). This suggests that *Zeb2*-deficient Schwann cells exit the cell cycle normally and survive in the absence of myelination.

At all time points studied (including 1 year of age), we found no evidence for axonal degeneration, except for rare axonal swellings (data not shown). At 1 year, the total number of axons was unaltered in mutants compared to controls (**Supplementary Fig. 1c**,**d**). This suggests that *Zeb2*-deficient Schwann cells can support axon survival despite a dysmyelination that causes conduction blocks.

Mutant Schwann cells express negative regulators of differentiation

To further define the stage at which *Zeb2*-deficient Schwann cells arrest in development, we performed a transcriptome analysis of sciatic nerves at age P25. Steady-state levels of more than 700 mRNAs differed at least twofold in abundance between the two genotypes. The top 20 upregulated and downregulated genes are shown in **Figure 3a**. We confirmed a subset of differentially regulated genes by quantitative real-time PCR, selecting promyelinating factors as well as negative regulators of myelination (**Fig. 3b**,**c**). As predicted from the phenotype of *Zeb2*-conditional mutants and the histological analysis, genes encoding myelin proteins were downregulated in mutants compared to controls (**Fig. 3c**). This was also the case for promyelinating factors of PNS myelination, such as Oct6 and Krox20 (**Fig. 3c**). Notably, *Zeb2*-deficient Schwann cells revealed the persistent expression of transcripts that are normally downregulated at this age (**Fig. 3b**). This includes transcripts for negative regulators of Schwann cell differentiation (for example, Sox2, c-Jun, Id2) and markers defining immature Schwann cells (for example, Gfap). *Zeb2*-deficient Schwann cells also expressed very low amounts of S100β, a well-known marker of both immature and mature Schwann cells (**Fig. 3c**). In addition, we identified the Notch effector *Hey2* as one of the most strongly (16.7 ± 1.4-fold) upregulated genes in our data set (**Fig. 3a**,**b**), as confirmed by quantitative PCR (qPCR). Other components of the Notch signaling cascade were also upregulated in our microarray analysis in mutants compared to controls, such as Notch1 (1.3-fold), Hes1 (1.6-fold) and Jagged1 (1.9-fold), arguing for persistently activated inhibitory Notch signaling in *Zeb2*-deficient Schwann cells. Using qPCR, we also found and confirmed highly elevated (13.4 ± 3.1-fold) expression of the endothelin receptor B (*Ednrb*) gene (**Fig. 3b**), encoding an efficient repressor of Schwann cell differentiation upon ligand binding[31]. Taken together, these facts suggest that *Zeb2*-deficient Schwann cells are arrested at an early developmental stage, with a very low expression of maturation factors and persistent (abnormal) expression of several negative regulators.

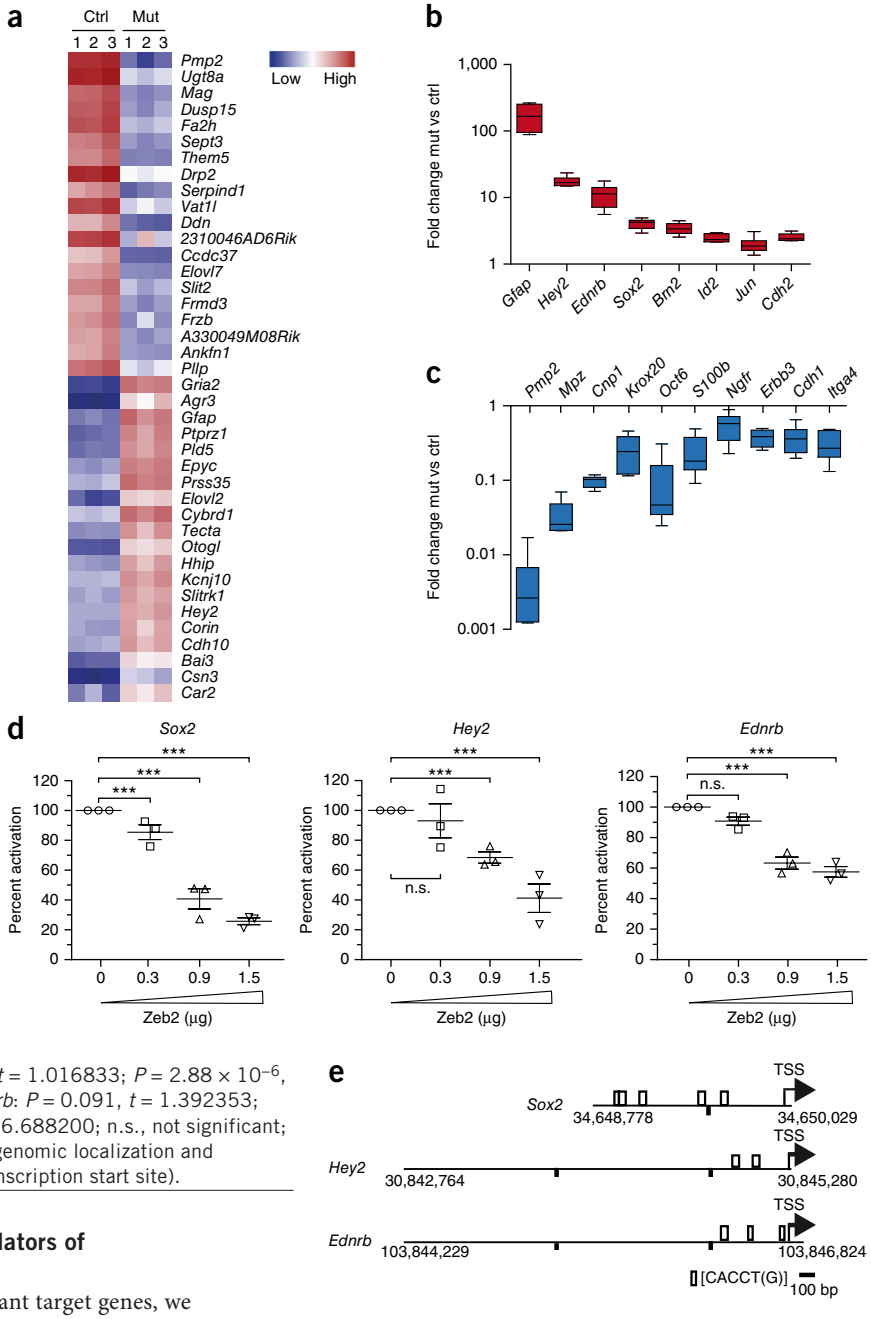

Figure 3 *Zeb2*-deficient Schwann cells continuously express developmental inhibitors. (**a**) Heat map of a microarray analysis depicting the 20 most up- and downregulated genes in sciatic nerves of 3 *Dhh-cre*::*Zeb2*$^{loxP/loxP}$ mice (Mut) compared to littermate controls (Ctrl) at age P25. (**b**,**c**) A subset of promyelinating factors and developmental inhibitors was confirmed by quantitative real-time PCR. Note the logarithmic scale. $n = 6$ animals per genotype, except *Gfap* ($n = 3$ mutants and 4 controls), two-sided Student's *t*-test of unpaired samples. *Gfap* $P = 0.026$, $t = 3.461$; *Hey2* $P = 4.57 \times 10^{-5}$, $t = 12.67411$; *Ednrb* $P = 0.002$, $t = 5.740$; *Sox2* $P = 1.4 \times 10^{-5}$, $t = 8.247414$; *Brn2* $P = 0.0006$, $t = 4.939481$; *Id2* $P = 0.0004$, $t = 5.430061$; *Jun* $P = 0.008$, $t = 4.013638$; *Cdh2* $P = 8.18 \times 10^{-6}$, $t = 8.972395$; *Pmp2* $P = 3.5 \times 10^{-5}$, $t = 13.80419$; *Mpz* $P = 0.0001$, $t = 9.639648$; *Cnp1* $P = 9.56 \times 10^{-5}$, $t = 11.06300$; *Krox20* $P = 0.002$, $t = 4.786690$; *Oct6* $P = 0.001$, $t = 6.015117$; *S100b* $P = 0.002$, $t = 4.855561$; *Ngfr* $P = 0.005$, $t = 3.579138$; *Erbb3* $P = 0.0003$, $t = 6.287818$; *Cdh1* $P = 0.0006$, $t = 5.291520$; *Itga4* $P = 0.0003$, $t = 6.020152$. Whiskers show minima and maxima; boxes extend from the first to the third quartiles with cross lines at the median. (**d**) Luciferase assays revealing *Zeb2* gene dosage-dependent reduction of promoter activity of *Sox2*, *Hey2* and *Ednrb* in S16 cells upon cotransfection with a Zeb2 expression plasmid. Each data point represents 1 independent experiment with 3 replicates ± s.e.m. with cross lines at the mean. Activity of lysates from cells cotransfected with the plasmid containing the respective promoter fragment and the empty pCMV5 plasmid was considered 100%. ($n = 3$ independent experiments with 3 replicates, one-sided Student's *t*-test of unpaired samples; versus 0 µg, from left to right: *Sox2*: $P = 0.0005$, $t = 3.977938$; $P = 2.89 \times 10^{-11}$, $t = 15.28166$; $P = 1.46 \times 10^{-14}$, $t = 25.04342$; *Hey2*: $P = 0.162$, $t = 1.016833$; $P = 2.88 \times 10^{-6}$, $t = 6.631628$; $P = 2.16 \times 10^{-8}$, $t = 9.678931$; *Ednrb*: $P = 0.091$, $t = 1.392353$; $P = 2.48 \times 10^{-5}$, $t = 5.488391$, $P = 2.6 \times 10^{-6}$, $t = 6.688200$; n.s., not significant; $^{***}P < 0.001$). (**e**) Promoter fragments with murine genomic localization and predicted Zeb2 binding sites (as used in **d**); TSS, transcription start site).

Schwann cell Zeb2 represses negative regulators of differentiation

To test whether Zeb2 acts as a repressor of relevant target genes, we performed luciferase gene reporter assays using the S16 Schwann cell line (**Fig. 3d**). Promoter regions of murine *Sox2*, *Hey2* and *Ednrb*, each containing putative Zeb2 (E-box-like) binding sites[17] (**Fig. 3e**), were cloned into the pGL2 luciferase plasmid and cotransfected with increasing amounts of a Zeb2 expression plasmid into S16 cells. This led to a significant dose-dependent downregulation of luciferase activity when compared to cotransfection with empty pCMV5 plasmid set to 100% (**Fig. 3d**). To confirm the interaction of Zeb2 and its target genes at the DNA level, we performed chromatin immunoprecipitation (ChIP) experiments using pooled sciatic nerves from 1-d-old wild-type mice. By qPCR, we detected an enrichment of amplified fragments from the promoters of all three target genes (*Sox2*, *Hey2* and *Ednrb*) that contained the canonical Zeb2 binding site, compared to control ChIP experiments without the Zeb2 antibody (**Supplementary Fig. 2**). A DNA fragment of a bona fide target gene (*Cdh1*) lacking a Zeb2 recognition site was used as a negative control.

Zeb2-mediated repression of Ednrb and Hey2 *in vivo*

To determine whether Zeb2-mediated inhibition of inhibitors is also functionally relevant *in vivo*, we generated double mutant mice that combined *Zeb2* deletion with the loss of either *Ednrb* or *Hey2*, for which *loxP*-flanked alleles were available[32,33]. By crossbreeding, we obtained two genotypes (*Dhh-cre*::*Zeb2*$^{loxP/loxP}$::*Ednrb*$^{loxP/loxP}$ and *Dhh-cre*::*Zeb2*$^{loxP/loxP}$::*Hey2*$^{loxP/loxP}$), hereafter called Zeb2/Ednrb-dcKO and Zeb2/Hey2-dcKO. As phenotypic rescue was not expected with the loss of only one inhibitor, we searched for histological signs of improvement in these double mutants. We immunostained cross-sections of sciatic nerves for Krox20. The number of labeled Schwann cell nuclei seen in *Zeb2*$^{loxP/loxP}$ controls (36.7 ± 2.9 per section; **Fig. 1c**) was strongly reduced in *Zeb2* single mutants (to 6.0 ± 0.4), but increased significantly both in Zeb2/Ednrb-dcKO (to 19.9 ± 4.3) and in Zeb2/Hey2-dcKO (to 16.8 ± 2.9) sciatic nerves (**Fig. 4a**,**b**).

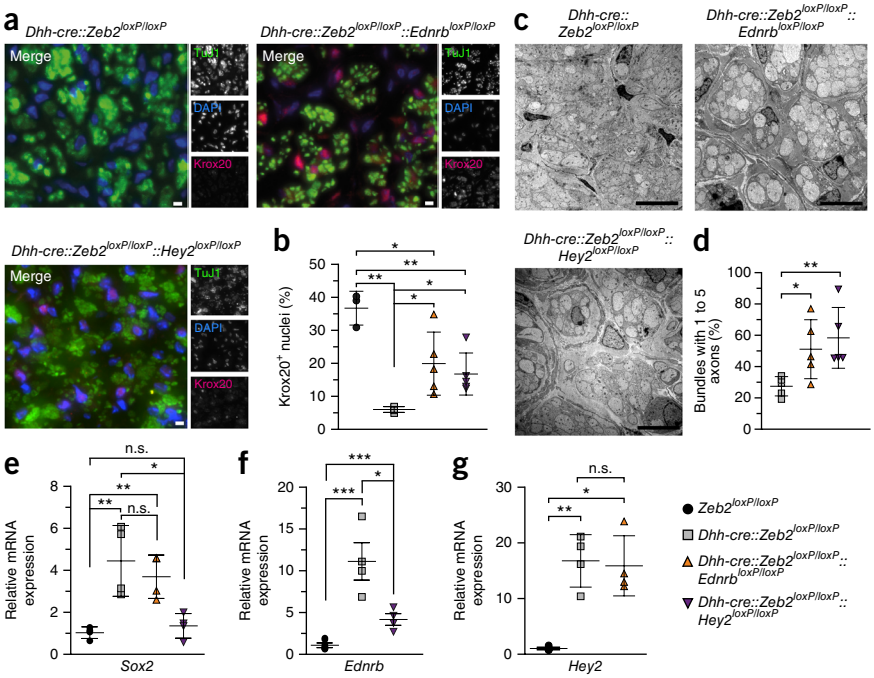

Figure 4 Zeb2-mediated repression of *Ednrb* and *Hey2* is functionally relevant. (**a**) Virtual absence of Krox20 from *Zeb2* conditional knockout Schwann cells (upper left) and reemergence in a subpopulation of Schwann cells in both Zeb2/Ednrb-dcKO (upper right) and Zeb2/Hey2-dcKO (lower left). Green, axons (TuJ1); blue, Schwann cell nuclei (DAPI); red, Krox20. Scale bars, 5 µm. The experiment was successfully repeated with sections from 5 animals per genotype (except $Zeb2^{loxP/loxP}$ $n = 3$ and $Dhh\text{-}cre::Zeb2^{loxP/loxP}$ $n = 4$) and representative images are shown. (**b**) Quantification of the Krox20-positive nuclei shown in **a**. Each data point represents one individual animal ± s.d. with cross lines at the mean; $n = 5$ animals per genotype (except $Zeb2^{loxP/loxP}$ $n = 3$ and $Dhh\text{-}cre::Zeb2^{loxP/loxP}$ $n = 4$). $Zeb2^{loxP/loxP}$ vs. $Dhh\text{-}cre::Zeb2^{loxP/loxP}$, $P = 0.008$, $t = 12.17175$; $Dhh\text{-}cre::Zeb2^{loxP/loxP}$ vs. $Dhh\text{-}cre::Zeb2^{loxP/loxP}::Ednrb^{loxP/loxP}$, $P = 0.03$, $t = 2.858292$; $Dhh\text{-}cre::Zeb2^{loxP/loxP}$ vs. $Dhh\text{-}cre::Zeb2^{loxP/loxP}::Hey2^{loxP/loxP}$, $P = 0.013$, $t = 3.299356$; $Zeb2^{loxP/loxP}$ vs. $Dhh\text{-}cre::Zeb2^{loxP/loxP}::Hey2^{loxP/loxP}$ $P = 0.004$, $t = 4.564169$, $Zeb2^{loxP/loxP}$ vs. $Dhh\text{-}cre::Zeb2^{loxP/loxP}::Ednrb^{loxP/loxP}$, $P = 0.03$, $t = 2.760013$ (two-sided Student's *t*-test of unpaired samples). (**c**) Improved radial sorting and smaller axon bundles in sciatic nerves of conditional Zeb2/Ednrb-dcKO (upper right) and Zeb2/Hey2-dcKO (lower left) double mutant mice compared to conditional *Zeb2* single mutants (upper left) at age P25. Scale bars, 5 µm. Representative of 5 mice per genotype. (**d**) Higher number of bundles with only 1 to 5 axons per Schwann cell in both double mutant mice at age P25 compared to *Zeb2* single mutants; $n = 5$ animals per genotype (on average 26 randomly chosen bundles per animal; each data point represents the mean percentage of bundles from one individual animal ± s.d. with cross lines at the mean). $Dhh\text{-}cre::Zeb2^{loxP/loxP}$ vs. $Dhh\text{-}cre::Zeb2^{loxP/loxP}::Ednrb^{loxP/loxP}$, $P = 0.0283$, $t = 2.670897$; $Dhh\text{-}cre::Zeb2^{loxP/loxP}$ vs. $Dhh\text{-}cre::Zeb2^{loxP/loxP}::Hey2^{loxP/loxP}$, $P = 0.0031$, $t = 4.185530$ (two-sided Student's *t*-test of unpaired samples). (**e**) *Sox2* expression at age P25 was significantly upregulated in $Dhh\text{-}cre::Zeb2^{loxP/loxP}$ mice and $Dhh\text{-}cre::Zeb2^{loxP/loxP}::Ednrb^{loxP/loxP}$ mice, but not in $Dhh\text{-}cre::Zeb2^{loxP/loxP}::Hey2^{loxP/loxP}$ mice, compared to $Zeb2^{loxP/loxP}$ mice. $Zeb2^{loxP/loxP}$ vs. $Dhh\text{-}cre::Zeb2^{loxP/loxP}$, $P = 0.0071$, $t = 3.999399$; $Dhh\text{-}cre::Zeb2^{loxP/loxP}$ vs. $Dhh\text{-}cre::Zeb2^{loxP/loxP}::Ednrb^{loxP/loxP}$, $P = 0.480$, $t = 0.7625912$; $Dhh\text{-}cre::Zeb2^{loxP/loxP}$ vs. $Dhh\text{-}cre::Zeb2^{loxP/loxP}::Hey2^{loxP/loxP}$, $P = 0.0133$, $t = 3.467755$; $Zeb2^{loxP/loxP}$ vs. $Dhh\text{-}cre::Zeb2^{loxP/loxP}::Hey2^{loxP/loxP}$, $P = 0.3598$, $t = 0.9913170$; $Zeb2^{loxP/loxP}$ vs. $Dhh\text{-}cre::Zeb2^{loxP/loxP}::Ednrb^{loxP/loxP}$, $P = 0.0025$, $t = 4.978021$ ($n = 4$ mice per genotype, two-sided Student's *t*-test of unpaired samples). (**f**) *Ednrb* expression at age P25 was significantly upregulated in $Dhh\text{-}cre::Zeb2^{loxP/loxP}$ mice and $Dhh\text{-}cre::Zeb2^{loxP/loxP}::Hey2^{loxP/loxP}$ mice compared to controls ($n = 4$ $Zeb2^{loxP/loxP}$ mice and 4 $Zeb2^{loxP/loxP}::Hey2^{loxP/loxP}$ mice). Expression in $Dhh\text{-}cre::Zeb2^{loxP/loxP}::Hey2^{loxP/loxP}$ mice was significantly lower than in $DhhCre::Zeb2^{loxP/loxP}$ mice ($n = 4$ mice per genotype: controls vs. $Dhh\text{-}cre::Zeb2^{loxP/loxP}$, $P = 2.5588 \times 10^{-5}$, $t = 7.314075$; $Dhh\text{-}cre::Zeb2^{loxP/loxP}$ vs. $Dhh\text{-}cre::Zeb2^{loxP/loxP}::Hey2^{loxP/loxP}$, $P = 0.0163$, $t = 3.303197$; controls vs. $Dhh\text{-}cre::Zeb2^{loxP/loxP}::Hey2^{loxP/loxP}$, $P = 9.4176 \times 10^{-5}$, $t = 6.257124$; two-sided Student's *t*-test of unpaired samples). (**g**) *Hey2* expression at age P25 was significantly higher in $Dhh\text{-}cre::Zeb2^{loxP/loxP}::Ednrb^{loxP/loxP}$ mice compared to controls ($n = 4$ $Zeb2^{loxP/loxP}$ mice and 4 $Zeb2^{loxP/loxP}::Ednrb^{loxP/loxP}$ mice) and not significantly different from $Dhh\text{-}cre::Zeb2^{loxP/loxP}$ mice: controls vs. $Dhh\text{-}cre::Zeb2^{loxP/loxP}$, $P = 0.00676$, $t = 9.932308$; $Dhh\text{-}cre::Zeb2^{loxP/loxP}$ vs. $Dhh\text{-}cre::Zeb2^{loxP/loxP}::Ednrb^{loxP/loxP}$, $P = 0.8133$, $t = 0.2467216$; controls vs. $Dhh\text{-}cre::Zeb2^{loxP/loxP}::Ednrb^{loxP/loxP}$, $P = 0.047$, $t = 8.177906$ ($n = 4$ mice per genotype, two-sided Student's *t*-test of unpaired samples, $^*P < 0.05$; $^{**}P < 0.01$; $^{***}P < 0.001$; n.s., not significant.).

At the morphological level, axon–Schwann cell units also appeared more mature in Zeb2/Ednrb-dcKO and Zeb2/Hey2-dcKO mice, at least when compared to the large and unsorted fiber bundles of *Zeb2* single mutants (**Fig. 4c**). The number of Remak-like (partially sorted) bundles with only 1–5 axons at age P25 (**Fig. 4d**) was higher in sciatic nerve cross-sections of double mutants (Zeb2/Ednrb-dcKO: 51.1 ± 18.85%; Zeb2/Hey2-dcKO: 55.2 ± 13.49%) than *Zeb2* single mutants ($Dhh\text{-}cre::Zeb2^{loxP/loxP}$: 27.5 ± 6.1%). Thus, the lack of one negative regulator (downstream of Zeb2) improved the ability of *Zeb2*-mutant Schwann cells to initiate axon sorting. To further characterize Zeb2/Ednrb-dcKO and Zeb2/Hey2-dcKO mutants, we analyzed target gene expression in sciatic nerves at age P25 (**Fig. 4e–g**). We did not detect any change in *Sox2* or *Hey2* mRNA in Zeb2/Ednrb-dcKO mice in comparison to controls ($Zeb2^{loxP/loxP}$ mice in **Fig. 4e** and $Zeb2^{loxP/loxP}::Ednrb^{loxP/loxP}$ mice in **Fig. 4g**) However, Sox2 levels were significantly lower in Zeb2/Hey2-dcKO mice than in $Dhh\text{-}cre::Zeb2^{loxP/loxP}$ mice and were comparable to $Zeb2^{loxP/loxP}$ mice (**Fig. 4e**). Ednrb was also significantly downregulated in comparison to $Zeb2^{loxP/loxP}$ single mutants (**Fig. 4f**).

Zeb2-deficient Schwann cells fail to efficiently support regeneration

Since Schwann cells re-expressed Zeb2 after an acute nerve injury (**Fig. 1b**), we asked whether the induction of Schwann cell dedifferentiation and peripheral nerve regeneration would be affected by the absence of Zeb2. To this end, we inactivated *Zeb2* in Schwann cells of adult mice, using a tamoxifen-inducible *Plp1-creERT2* driver line[34]. Recombination was induced at 6–8 weeks of age and efficient CreERT2 expression was confirmed on sciatic nerve cryostat sections using a Cre-sensitive tdTomato reporter allele[35] (**Supplementary Fig. 3**).

When $Plp1\text{-}creERT2::Zeb2^{loxP/loxP}$ mice were analyzed 12 weeks after the last tamoxifen injection, sciatic nerve morphology and myelin sheath thickness appeared unaltered (**Supplementary Fig. 4a,b**). We then performed sciatic nerve crushes in mice 4 weeks after the last tamoxifen or vehicle injection. Footprint sequences of walking mice were used to monitor functional recovery. For histological analyses, animals were sacrificed 11, 28 and 56 days after sciatic nerve crush. In these experiments, mice from the three control groups functionally

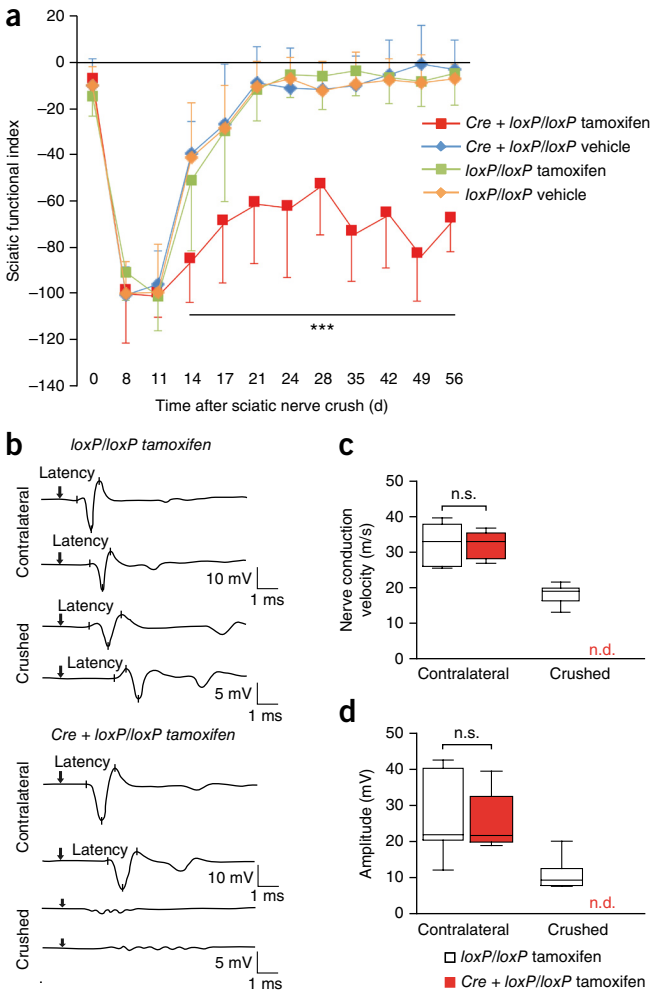

Figure 5 Zeb2 is required for efficient recovery after nerve injury. (**a**) Functional recovery after nerve crush is significantly perturbed in tamoxifen-treated *Plp1-creERT2::Zeb2*$^{loxP/loxP}$ mice (Cre + *loxP/loxP* tamoxifen, red) in comparison to three control groups, as determined by the sciatic functional index. Data points depict mean ± s.d., $n \geq 10$ animals per group (one-way ANOVA, day 0: $P = 0.3064$, $F_{3,38} = 1.246703$; day 8: $P = 0.3577$, $F_{3,39} = 1.107561$; day 11 $P = 0.8386$, $F_{3,44} = 0.2813102$; day 14 $P = 0.0001$, $F_{3,39} = 8.903$; day 17 $P = 0.0001$, $F_{3,45} = 8.481348$; day 21 $P = 4.23781 \times 10^{-10}$, $F_{3,46} = 26.47369$; day 24, $P = 1.52347 \times 10^{-8}$, $F_{3,37} = 22.85789$, day 28, $P = 6.29699 \times 10^{-9}$, $F_{3,41} = 23.14702$; day 35 $P = 3.00629 \times 10^{-14}$, $F_{3,40} = 54.95588$; day 42, $P = 5.11929 \times 10^{-12}$, $F_{3,41} = 38.61261$; day 49, $P = 4.01117 \times 10^{-16}$, $F_{3,40} = 71.49940$; day 56 $P = 7.98803 \times 10^{-15}$, $F_{3,39} = 61.31167$; $^{***}P < 0.001$). (**b**) Electrophysiological recordings of CMAPs after sciatic nerve stimulation 52 d after crush injury. Note the persistent conduction blocks in tamoxifen-treated *Plp1-creERT2::Zeb2*$^{loxP/loxP}$ mice (bottom), in contrast to control nerves (top) that regained functional nerve conduction. Representative traces of 8 *Zeb2*$^{loxP/loxP}$ tamoxifen-treated mice and 5 *Plp1-creERT2::Zeb2*$^{loxP/loxP}$ tamoxifen-treated mice are shown. (**c**) Nerve conduction velocity was regained to about 54% in control nerves but could not be determined (n.d.) in conditional *Zeb2* mutants. Whiskers show minima and maxima; boxes extend from the first to the third quartiles with cross lines at the median. (tamoxifen-treated *Zeb2*$^{loxP/loxP}$: $n = 7$ animals, tamoxifen-treated *Plp1-creERT2::Zeb2*$^{loxP/loxP}$ animals: $n = 5$, two-sided Student's *t*-test of unpaired samples $P = 0.8737$, $t = 0.16361498$; n.s., not significant). (**d**) CMAP amplitudes as a measure of functional renervation were partly restored in control mice but remained undetectable (n.d.) in conditional *Zeb2* mutants. Whiskers show minima and maxima; boxes extend from the first to the third quartiles with cross lines at the median (tamoxifen-treated *Zeb2*$^{loxP/loxP}$: $n = 7$ animals, tamoxifen-treated *Plp1-creERT2::Zeb2*$^{loxP/loxP}$ animals: $n = 5$, two-sided Student's *t*-test of unpaired samples $P = 0.9022$, $t = 0.1260085$; n.s., not significant).

recovered as expected and as measured by the sciatic functional index. However, *Plp1-creERT2::Zeb2*$^{loxP/loxP}$ mice remained severely impaired until the end of this study (56 d after crush; **Fig. 5a**).

In physiological tests carried out 52 d after sciatic nerve crush, *Zeb2*$^{loxP/loxP}$ control mice regained significant motor nerve conduction. We recorded a nerve conduction velocity (NCV) of about 18 ± 2.9 m/s, which is about 54% of the NCV of an unharmed contralateral nerve (33 ± 5.2 m/s), as determined in mice of either genotype. In contrast, *Zeb2* conditional mutants maintained severe axonal conduction problems that did not allow us to measure any NCV (**Fig. 5b**,**c**). Distal amplitudes (normal contralateral nerve: 29.8 ± 10.1 mV) were still reduced 52 d after crush injury in control mice (10.9 ± 4.4 mV) and undetectable in *Plp1-creERT2::Zeb2*$^{loxP/loxP}$ mutants, indicating a regeneration failure with irreversible conduction blocks (**Fig. 5d**).

Indeed, when we immunostained sciatic nerve cross-sections for myelin (Mbp) and axons (TuJ1), virtually all fibers showed remyelination in control mice (**Fig. 6a**), whereas in nerves of tamoxifen-induced *Plp1-creERT2::Zeb2*$^{loxP/loxP}$ mutants we observed large amyelinated fibers 8 weeks after injury (**Fig. 6a**). We also analyzed remyelination by electron microscopy (**Fig. 6b**,**c**,**e**). At 28 d and 56 d after crush injury, mutants exhibited significantly fewer remyelinated axons (**Fig. 6d**,**e** and **Supplementary Fig. 5a**).

Interestingly, remyelinated axons in mutant (*Plp1-creERT2::Zeb2*$^{loxP/loxP}$) mice had the same myelin sheath thickness as in the three respective control groups (*Zeb2*$^{loxP/loxP}$ mice lacking either *Plp1-creERT2*, tamoxifen or both), as measured by G-ratio analysis (**Supplementary Fig. 5b**). Additionally, 56 d after crush we still observed remyelinating Schwann cells with myelin loops that were fewer in number and uncompacted (**Fig. 6b**). Thus, the timing of Zeb2 re-expression after acute nerve trauma (**Fig. 1b**) and the defect of remyelination in mutant mice strongly suggest Zeb2 is key to efficient Schwann cell response upon nerve injury.

Zeb2-deficient Schwann cells do not fully redifferentiate

To distinguish between alternative Zeb2 functions after nerve injury, we first studied sciatic nerves in tamoxifen-treated *Plp1-creERT2::Zeb2*$^{loxP/loxP}$ mice 3 d after transection, when Schwann cell dedifferentiation is at its peak. At this time, there was no significant difference in the number of residual myelin sheaths (1,650 ± 89 per section), when compared with vehicle-treated controls (1,785 ± 287), 3.0 mm distal to the transection site (**Fig. 7a**,**b**). We also detected no significant difference in the number of c-Jun-positive nuclei between two control groups and tamoxifen-treated mutants in distal segments of sciatic nerves 3 d after crush injury (**Fig. 7c**,**d**).

Moreover, steady-state mRNA levels of Schwann cell dedifferentiation markers[1] such as c-Jun, Sox2 and Ngfr were comparable in mutants and controls in the distal stump (**Fig. 7e** and data not shown), whereas myelination markers, such as Krox20 and Mpz, were downregulated in both mutants and controls compared to expression levels in the contralateral nerve (**Fig. 7e**). Taken together, these results indicate that the early steps of Schwann cell dedifferentiation are not perturbed by the lack of Zeb2.

We next analyzed at a functional level the regenerative axon outgrowth of crushed sciatic nerves in conditional *Zeb2* mutants and controls, using a pinch test. When tested 4 d after injury, deeply anesthetized mice of all three control groups showed a clear muscle

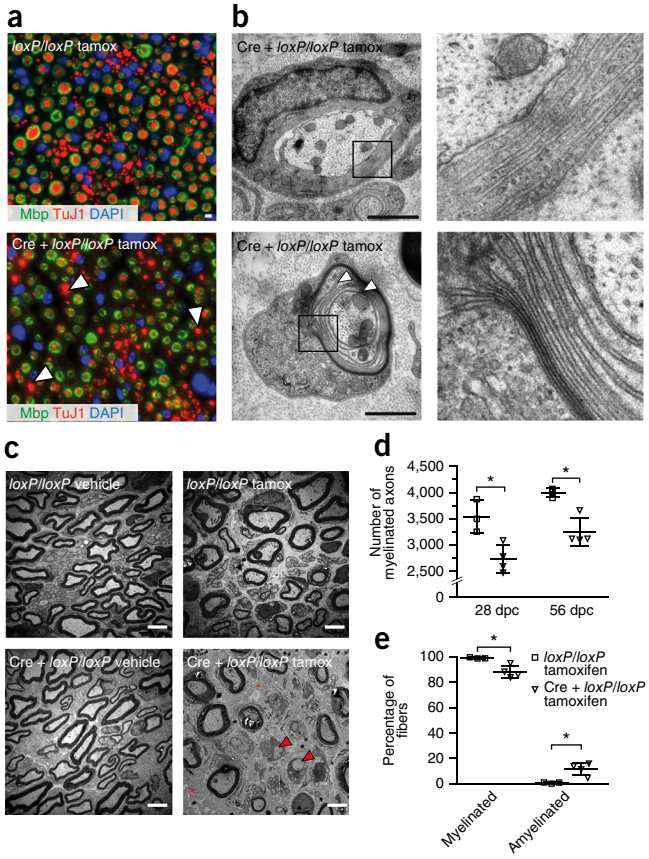

Figure 6 Remyelination by *Zeb2*-deficient Schwann cells is impaired. (**a**) In contrast to control mice 56 d after sciatic nerve crush injury (top), tamoxifen-treated *Plp1-creERT2::Zeb2*$^{loxP/loxP}$ mice (bottom) have many amyelinated fibers remaining (white arrowheads), as visualized by staining axons (TuJ1, red) and myelin sheaths (Mbp, green). The experiment was successfully repeated with sections from 3 animals per group and representative images (see also quantification in **d**) are shown. Scale bar, 5 µm. (**b**) Fifty-six days after nerve crush mutant mice still exhibit signs of ongoing remyelination, such as cytoplasm-filled myelin wraps (top) and thinly compact sheaths (bottom). Boxed areas are magnified to the right. Scale bars, 1 µm. (**c**) In contrast to various controls that regenerate well, tamoxifen-treated *Plp1-creERT2::Zeb2*$^{loxP/loxP}$ mice (bottom right) exhibit axon-free fibrotic areas (asterisks) and unmyelinated axons (arrowheads). Scale bars, 2.5 µm. Electron micrographs in panels **b** and **c** are representative of 4 animals per treatment and genotype. (**d**) Impaired axonal regeneration and remyelination in mutant mice. Note that fewer myelinated axons (>1 µm) are seen 28 d and 56 d after sciatic nerve crush on semi-thin sections. Each data point represents 1 individual mouse ± s.d. (tamoxifen-treated *Zeb2*$^{loxP/loxP}$: $n = 3$, tamoxifen-treated *Plp1-creERT2::Zeb2*$^{loxP/loxP}$: $n = 4$, two-tailed Student's *t*-test of unpaired samples, 28 days: $P = 0.014$, $t = 3.697461$; 56 days: $P = 0.0063$, $t = 4.520971$; $^*P < 0.05$). (**e**) Confirmation at the electron microscopy level (56 dpc), where amyelinated axons can be clearly visualized (same animals as in **d**). Each data point represents 1 individual mouse ± s.d. (25 randomly chosen electron micrographs at 3,000× magnification per animal, amyelinated $P = 0.0137$, $t = 3.721040$; myelinated $P = 0.0137$, $t = 3.721040$, two-tailed Student's *t*-test of unpaired samples, $^*P < 0.05$).

reaction to a pinch of the sciatic nerve applied with a pair of forceps distal to the original crush site (**Fig. 7f**). However, the distance at which a response could be elicited differed between genotypes, indicating more efficient axon outgrowth in all control groups (for example, 6.6 ± 0.8 mm in mice lacking Cre) compared to tamoxifen-treated *Zeb2* mutants (5.4 ± 1.3 mm).

We hypothesized that reduced regenerative capacity is caused by poor Schwann cell differentiation. We therefore analyzed the distal stump of sciatic nerves at a late time point (56 d after crush), when control mice had fully recovered. Indeed, in *Zeb2* mutants we could still detect a significant expression of dedifferentiation markers, such as Sox2 and Id2 (**Fig. 7g**). Notably, *Hey2* mRNA was only upregulated in mutant nerves (**Fig. 7g**) (i.e., there was ectopic expression similar to that found in *Zeb2*-deficient Schwann cells at age P25). In contrast, *Krox20* was downregulated only in mutant nerves (in comparison to the sustained expression in uninjured nerves), whereas *Oct6* expression levels were similar in mutants and controls (**Fig. 7g**). Taken together, these data indicate that *Zeb2*-deficient Schwann cells can dedifferentiate after injury, but fail to redifferentiate and provide efficient myelin repair.

DISCUSSION

We have identified an essential regulator of Schwann cell differentiation and peripheral myelination, the two-handed zinc finger/homeodomain protein Zeb2. In contrast to previously described promyelinating transcription factors in the Schwann cell lineage, such as Oct6, Krox20 and Sox10, which activate the transcription of downstream factors and ultimately myelin-associated genes, Zeb2 is widely expressed[17] and a transcriptional repressor in Schwann cells. These findings are in agreement with the work of Wu *et al.*[36] (this issue).

Null mutant mice for *Sox10*, a gene which is, like *Zeb2*, expressed in the emerging neural crest, die embryonically with a lack of peripheral glia[8]. Later cell-specific deletion of *Sox10* after Schwann cell specification (induced by *Dhh-cre* as in *Zeb2* conditional knockout mice) leads to a similar developmental arrest in peripheral nerves with a lack of radial axonal sorting and virtual absence of myelin[9].

Early arrest of Schwann cell maturation has been observed before in the context of chromatin remodeling. Mice in which Schwann cells lack *Brg1*, encoding a subunit of the Brg1/Brm-associated factors (BAF) chromatin-remodeling complex that is recruited by Sox10, develop a severe peripheral neuropathy and die prematurely[37]. Whereas the morphological defects of dysmyelination are strikingly similar in conditional *Dhh-cre::Sox10*, *Dhh-cre::Brg1* and *Dhh-cre::Zeb2* mutant mice, in *Zeb2*-deficient mice all Schwann cells survive. Despite the virtual absence of myelin and similarly severe neuropathy, conditional *Zeb2*-mutant mice have a normal life span, and *Zeb2*-deficient Schwann cells support axon survival. Apparently the (ancestral) function of axon-ensheathing glial cells in providing metabolic support is maintained.

We also note that in *Zeb2*-deficient Schwann cells *Sox10* mRNA itself is unaltered in abundance (data not shown). The transcriptional (co-)activator Sox10 is expressed throughout the Schwann cell lineage and directly binds to Oct6 and Krox20, potentially affecting a broader set of myelin-associated genes[6], most likely including those that are required for survival and axonal metabolic support. We speculate that Schwann cell–mediated axonal support, which protects against complete paralysis and lethal breathing defects, is largely independent of Zeb2.

The developmental defect of conditional *Zeb2*-mutant mice is more severe than those of *Oct6* or *Krox20* mutants. Deletion of *Oct6* causes only a transient arrest of Schwann cell differentiation after radial sorting; i.e., at the promyelin stage[38,39]. Likewise, Schwann cells lacking *Krox20* are able to sort axons but then completely fail to myelinate[4].

Considering the unaltered levels of *Sox10* mRNA in *Zeb2*-deficient Schwann cells and the more severe phenotype than that observed in *Krox20*-null mice, the most likely explanation why conditional

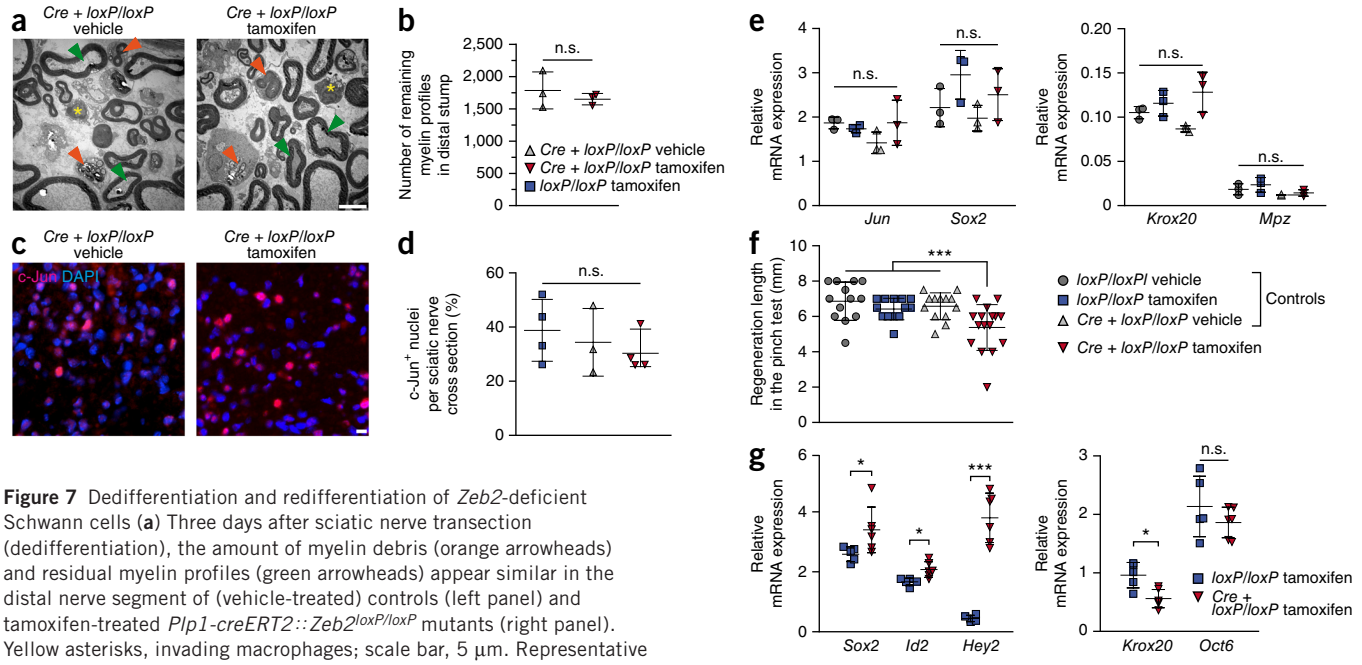

Figure 7 Dedifferentiation and redifferentiation of *Zeb2*-deficient Schwann cells (**a**) Three days after sciatic nerve transection (dedifferentiation), the amount of myelin debris (orange arrowheads) and residual myelin profiles (green arrowheads) appear similar in the distal nerve segment of (vehicle-treated) controls (left panel) and tamoxifen-treated *Plp1-creERT2::Zeb2*$^{loxP/loxP}$ mutants (right panel). Yellow asterisks, invading macrophages; scale bar, 5 µm. Representative images of 3 mice per group. (**b**) When quantified in the distal sciatic nerve stump, the number of residual myelin profiles is not different (each data point represents 1 individual animal ± s.d., $P = 0.50456$, $t = 0.7819589$, $n = 3$ mice per group, two-sided Student's *t*-test of unpaired samples; n.s., not significant). (**c**) Nuclear c-Jun immunofluorescence on cross-sections of the distal sciatic nerve segment 3 d after nerve crush shows a similar number of dedifferentiating Schwann cells (c-Jun, pink; DAPI, blue; the experiment was repeated successfully on sections of 4 mice per group, except for Cre + *loxP/loxP* vehicle, for which $n = 3$; scale bar, 5 µm). (**d**) Quantification of c-Jun-positive nuclei on sections of the distal sciatic nerve segment 3 d after nerve crush as depicted in **c** shows a similar number for tamoxifen-treated *Plp1-creERT2::Zeb2*$^{loxP/loxP}$ mutants and two corresponding control groups ($n = 4$ mice per group, except for Cre + *loxP/loxP* vehicle for which $n = 3$; each data point represents one individual animal ± s.d.; one-way ANOVA, $P = 0.5366$, $F_{2,8} = 0.6735603$). (**e**) After 3 d, normal Schwann cell dedifferentiation is also suggested by the elevated steady-state levels of *Jun* and *Sox2* mRNAs. *Krox20* and *Mpz* mRNAs were similarly downregulated in all groups. Expression in the contralateral nerve was defined as 1.0. Each data point represents sciatic nerve mRNA from 1 individual mouse with cross lines at the mean ± s.d. ($n = 3$ mice per group, Kruskal-Wallis one-way ANOVA: *Jun*, $P = 0.1473$, $H = 5.358974$; *Sox2*, $P = 0.1319$, $H = 5.615385$; *Krox20*: $P = 0.0572$, $H = 7.512821$; *Mpz*: $P = 0.1129$, $H = 5.974$; n.s., not significant). (**f**) Delayed functional recovery of sciatic nerves after crush, as assessed by the pinch test reflecting axon regrowth. In tamoxifen-treated *Plp1-creERT2::Zeb2*$^{loxP/loxP}$ mice (red) regenerative length 4 d after nerve crush does not reach various control values (gray and blue). Each data point represents the regeneration distance of 1 individual mouse with cross lines at the mean ± s.d. ($n = 13$ mice per group except *loxP/loxP* tamoxifen, for which $n = 16$; one-way ANOVA: $P = 0.001$, $F_{3,51} = 6.356539$, $^{***}P = 0.001$). (**g**) After 56 d, levels of *Sox2* and *Id2* were strongly upregulated in injured nerves, but even more so in tamoxifen-treated *Plp1-creERT2::Zeb2*$^{loxP/loxP}$ mutant mice. *Hey2* levels were downregulated in injured control nerves, but highly upregulated in tamoxifen-treated *Plp1-creERT2::Zeb2*$^{loxP/loxP}$ mutant mice. *Krox20* levels remained low in nerves of mutants, while *Oct6* was still upregulated to comparable levels in both genotypes. Each data point represents cDNA from 1 individual mouse run in triplicate ± s.d. with cross lines at the mean. Expression in the contralateral nerve was defined as 1.0. (Cre + *loxP/loxP* tamoxifen, $n = 6$; *loxP/loxP* tamoxifen, $n = 5$; contralateral, $n = 5$. *Sox2*: $P = 0.0493$, $t = 2.271339$; *Id2*: $P = 0.0109$, $t = 3.197971$; *Hey2*: $P = 0.00072063$, $t = 8.963330$; *Krox20*: $P = 0.0062$, $t = 3.547758$; *Oct6*: $P = 0,2807$, $t = 1.147759$; $^{*}P < 0.05$; $^{***}P < 0.001$; n.s., not significant).

Zeb2-mutants display very low expression of Krox20 and myelin protein genes is not the absence of promyelin factors but the persistent presence of maturation inhibitors (for example, Sox2, c-Jun, Ednrb) and the resulting developmental arrest. However, we cannot formally exclude the possibility that transcriptional activation of unknown target genes by Zeb2 (for example, in combination with unknown coactivators) also promotes Schwann cell differentiation in wild-type mice. Details of the transcriptional repression mechanisms by Zeb2 remain to be determined. One possibility is an interaction of Zeb2 with the histone deacetylase 1/2 (HDAC1/2)–nucleosome remodeling deacetylase (NuRD) co-repressor complex[40] in Schwann cells[36].

With their radial sorting defect, conditional *Zeb2* mutants resemble mutants of basal lamina signaling, such as double conditional mutants for beta-1 integrin and dystroglycan[41] or laminin 2 and 8 double knockout mice[42]. In conditional *Zeb2* mutants, the basal lamina is thin, disorganized and often discontinuous. In dorsal root ganglion cocultures *Zeb2*-deficient Schwann cells failed to myelinate when provided with an artificial basal lamina (data not shown). Thus, basal lamina abnormalities are likely a secondary defect of *Zeb2*-deficient Schwann cells rather than the cause of dysmyelination.

We observed very low levels of *S100b* mRNA and S100β protein in *Zeb2*-deficient Schwann cells. This could mean that they are arrested even before reaching the immature developmental stage. However, this is unlikely, as we did not observe increased Schwann cell precursor proliferation or apoptosis.

The hierarchical relationship of the known transcription factors in the Schwann cell lineage is complex, owing in part to their broad temporal expression domains and changing molecular interactions, including positive feedback loops[3]. For example, *Krox20* is activated in promyelinating Schwann cells by the positive regulators Oct6 and Sox10, which then collectively upregulate genes for myelin proteins and enzymes of the lipid biosynthesis pathway. How are these feed-forward loops developmentally controlled? Our data on Zeb2 suggest the existence of several brakes in the system, with the loss of Zeb2 leading to continuous expression of developmental inhibitors that block axonal sorting and myelination. This group of negative regulators

overlaps but is not identical to other factors, such as c-Jun, known to drive programmed dedifferentiation of mature Schwann cells after nerve injury (see below).

By expression profiling of peripheral nerves from *Zeb2* mutant mice and by functional analysis of different promoter–reporter constructs, we identified *Ednrb*, *Sox2* and *Hey2* as target genes of Zeb2. We selected these genes from a much larger group of abnormally upregulated genes to show proof-of-principle for transcriptional repression by Zeb2, as well as for their putative inhibitory function in Schwann cell differentiation. Two of these genes had been previously associated with the Schwann cell lineage. Ednrb localizes to the plasma membrane of Schwann cell precursors and, upon binding of endothelin, delays the generation of immature Schwann cells both *in vitro* and *in vivo*. Indeed, *Ednrb* null mutant Schwann cells differentiate earlier than normal as shown by premature S100β expression[31].

Sox2 is also a member of the Sry-related high-mobility-group–box family of transcription factors, but (unlike Sox10) widely expressed. Sox2 is downregulated early in Schwann cell development, coinciding with Krox20 expression[43]. Recently, it has been found that overexpression of Sox2 (a transcriptional activator) leads to persistent proliferation of Schwann cells and inhibits myelination, implicating Sox2 as a negative regulator of Schwann cell maturation *in vivo* (D.B. Parkinson, personal communication).

Hey2, a member of the hairy and enhancer-of-split–related basic helix-loop-helix transcription factor family, recruits histone deacetylases to repress transcription and acts as a downstream effector of Notch signaling[44]. Notch signaling serves as a timer in the generation of immature Schwann cells from precursors and is downregulated in cells that express Krox20. Additionally, Notch acts as an inhibitor of myelination *in vitro* and *in vivo* and is re-expressed in the distal stump of cut nerves[45].

In our analysis, Hey2 was expressed at low levels in adult nerves and not activated during injury-induced Schwann cell dedifferentiation (**Fig. 7d** and data not shown). We found *Hey2* among the most highly upregulated mRNAs in sciatic nerves of *Dhh-cre::Zeb2*$^{loxP/loxP}$ mice at age P25. Moreover, Hey2 was strongly expressed in adult mutants 8 weeks after nerve injury. In both cases, ectopic induction of Hey2 was a special feature of *Zeb2*-deficient Schwann cells. The physiological function of Hey2 in the Schwann cell lineage remains unknown. The conditional *Dhh-cre::Hey2*$^{loxP/loxP}$ single mutants that we created in the course of our rescue experiments developed and myelinated normally (data not shown).

Thus, our findings suggest that negative regulatory proteins such as Sox2, Hey2 or Ednrb need to be downregulated early in development for Schwann cell differentiation, axonal sorting and myelination to proceed (**Supplementary Fig. 6**). Since Zeb2 itself is only transiently expressed, the downregulation of its target genes (inhibiting the inhibitors) most likely allows immature Schwann cells to overcome a developmental block, after which their further differentiation becomes Zeb2-independent. At least two of the identified Zeb2 target genes appear to contribute to this block (*Hey2* and *Ednrb*), as evident from the partial rescue in corresponding double-mutant mice. One cannot assume that the phenotype of *Zeb2* mutant mice can be rescued by introducing a second mutation into one gene for a (de-repressed) inhibitor. It is thus surprising that the additional deletion of either *Ednrb* or *Hey2* was sufficient to markedly increase the number of Krox20-positive Schwann cells and morphological signs of sorting (more bundles with only 1–5 axons) in corresponding double-mutant mice. Experiments to find out whether these effects can be strengthened by targeting yet other genes and combining them in triple and quadruple mutants are important but beyond the scope of this first report.

Normally myelinated (adult wild-type) nerves lack both Zeb2 and its repressed target gene product(s), strongly suggesting that other factors are responsible for maintaining the brake on the expression of inhibitors, which would otherwise trigger dedifferentiation. The identity of these repressors is not known. At the same time, myelin maintenance has been shown to depend on continuous expression of the promyelinating factors Sox10 and Krox20 (refs. 5,11).

Mutations of the human *ZEB2* gene cause the rare Mowat-Wilson syndrome, characterized by moderate to severe mental retardation, brain abnormalities and variable features including Hirschsprung disease[25]. A reduced response to nociceptive stimuli has been found in people affected by Mowat-Wilson syndrome[46], and lowered pain sensitivity and reduced number of nociceptive C-fibers have been demonstrated in *Zeb2* heterozygous null mice[47]. However, it is unclear whether the reduced pain response seen in some people with Mowat-Wilson syndrome is a peripheral neuropathy or CNS phenotype[46].

In the CNS, myelination by oligodendrocytes is controlled in many ways by negative regulators. Direct interactions with signaling molecules, such as bone morphogenetic protein (BMP), Notch ligand or Wnt proteins, can inhibit gene expression[48]. At the molecular level, chromatin remodeling and epigenetic silencing of transcriptional repressors also follows the inhibiting-the-inhibitors principle[49]. Zeb2 is also expressed in oligodendrocyte development, activated by Olig1 and Olig2, and is essential for CNS myelination as illustrated in *Olig-cre::Zeb2*$^{loxP/loxP}$ mice[23]. Zeb2 levels are low in oligodendrocyte precursors and high in mature oligodendrocytes, where Zeb2 serves a dual role as both a repressor and also as a transcriptional activator of the *Smad7* gene. The lack of Smad7 contributes to failed oligodendrocyte precursor differentiation and CNS dysmyelination in conditional mutant mice[23]. Thus, despite some phenotypic resemblances, Zeb2 serves different functions in PNS and CNS glial development.

When we deleted *Zeb2* in Schwann cells of adult mice, we found a severe delay in regeneration and functional recovery after sciatic nerve crush injury. Even after 8 weeks, remyelination was not complete. Such a dramatic failure of myelin repair has been described in mice lacking the AP1 transcription factor c-Jun in Schwann cells[50]. However, in *Jun* mutant mice, the formation of a functional repair cell is impaired, while in *Zeb2* conditional mutants, repair cells are generated but redifferentiation is inefficient. After sciatic nerve crush, Schwann cells lacking *Jun* fail to form regenerative tracts (bands of Büngner), which leads to a dramatic reduction of axon outgrowth[50]. Here we detected only a minor reduction in axon outgrowth when tested 4 d after crush (**Fig. 7e**). In *Zeb2* conditional mutants (and similarly to *Jun* conditional mutants), if remyelination does initiate, myelin repair proceeds normally, as determined by G-ratio analysis. It has been hypothesized that the so-called repair cell marks dedifferentiation beyond the immature Schwann cell stage[50]. One analysis of injured nerves even revealed Schwann cell–derived melanocytes, normally a distinct sublineage of precursor cells[51].

Repair cells that form after nerve injury and that are dependent on factors such as Zeb2 to fully activate the Schwann cell redifferentiation program are an important feature of nervous system function. Further characterization of genes involved in the plasticity of Schwann cells during development and in injury-related redifferentiation at adult stages will help to better understand the outcome of human demyelinating neuropathies and other diseases of the peripheral nervous system.

METHODS

Methods and any associated references are available in the online version of the paper.

Accession codes. GEO: microarray data, GSE76027.

Note: Any Supplementary Information and Source Data files are available in the online version of the paper.

ACKNOWLEDGMENTS

The authors would like to thank C. Maack, T. Durkaya and A. Fahrenholz for excellent technical assistance. We thank the staff of the Transcriptome Analysis Laboratory (TAL) of the University Medical Center Göttingen for performance and statistical analysis of the microarray analysis and A. Diedrich, M. Wehe, B. Nickel and T. Hoffmeister for excellent support in animal husbandry. We are grateful to Q.R. Lu for communicating unpublished data. M.W.S. is supported by a Heisenberg Professorship granted by the DFG (GZ: SE 1944/1-1). D.H. is supported by Belspo-IAP funding (IAPVII-07), FWO-V (G.0782.14), Hercules Foundation (ZW09-03 project InfraMouse) and Erasmus MC start-up funds. K.-A.N. is supported by the DFG (Research Center Molecular Physiology of the Brain, CNMPB) and holds a European Research Council Advanced Investigator Grant.

AUTHOR CONTRIBUTIONS

S.Q. and B.G.B. designed the study, performed experiments and wrote the manuscript. M.E., T.K. and F.A.A. contributed to the experiments. F.F. performed luciferase assays. V.T., D.H., D.M. and U.S. provided transgenic mice. M.W. supervised F.F. and contributed to discussions. M.W.S. and K.-A.N. contributed to the manuscript and supervised the study.

COMPETING FINANCIAL INTERESTS

The authors declare no competing financial interests.

1. Jessen, K.R. & Mirsky, R. Negative regulation of myelination: relevance for development, injury, and demyelinating disease. *Glia* **56**, 1552–1565 (2008).
2. Monk, K.R., Feltri, M.L. & Taveggia, C. New insights on Schwann cell development. *Glia* **63**, 1376–1393 (2015).
3. Stolt, C.C. & Wegner, M. Schwann cells and their transcriptional network: evolution of key regulators of peripheral myelination. *Brain Res.* http://dx.doi.org/10.1016/j.brainres.2015.09.025 (2015).
4. Topilko, P. *et al.* Krox-20 controls myelination in the peripheral nervous system. *Nature* **371**, 796–799 (1994).
5. Decker, L. *et al.* Peripheral myelin maintenance is a dynamic process requiring constant Krox20 expression. *J. Neurosci.* **26**, 9771–9779 (2006).
6. Ghislain, J. & Charnay, P. Control of myelination in Schwann cells: a Krox20 cis-regulatory element integrates Oct6, Brn2 and Sox10 activities. *EMBO Rep.* **7**, 52–58 (2006).
7. Kuhlbrodt, K., Herbarth, B., Sock, E., Hermans-Borgmeyer, I. & Wegner, M. Sox10, a novel transcriptional modulator in glial cells. *J. Neurosci.* **18**, 237–250 (1998).
8. Britsch, S. *et al.* The transcription factor Sox10 is a key regulator of peripheral glial development. *Genes Dev.* **15**, 66–78 (2001).
9. Finzsch, M. *et al.* Sox10 is required for Schwann cell identity and progression beyond the immature Schwann cell stage. *J. Cell Biol.* **189**, 701–712 (2010).
10. Fröb, F. *et al.* Establishment of myelinating Schwann cells and barrier integrity between central and peripheral nervous systems depend on Sox10. *Glia* **60**, 806–819 (2012).
11. Bremer, M. *et al.* Sox10 is required for Schwann-cell homeostasis and myelin maintenance in the adult peripheral nerve. *Glia* **59**, 1022–1032 (2011).
12. Le, N. *et al.* Nab proteins are essential for peripheral nervous system myelination. *Nat. Neurosci.* **8**, 932–940 (2005).
13. Desmazières, A., Decker, L., Vallat, J.M., Charnay, P. & Gilardi-Hebenstreit, P. Disruption of Krox20-Nab interaction in the mouse leads to peripheral neuropathy with biphasic evolution. *J. Neurosci.* **28**, 5891–5900 (2008).
14. Mager, G.M. *et al.* Active gene repression by the Egr2.NAB complex during peripheral nerve myelination. *J. Biol. Chem.* **283**, 18187–18197 (2008).
15. He, Y. *et al.* The transcription factor Yin Yang 1 is essential for oligodendrocyte progenitor differentiation. *Neuron* **55**, 217–230 (2007).
16. He, Y. *et al.* Yy1 as a molecular link between neuregulin and transcriptional modulation of peripheral myelination. *Nat. Neurosci.* **13**, 1472–1480 (2010).
17. Verschueren, K. *et al.* SIP1, a novel zinc finger/homeodomain repressor, interacts with Smad proteins and binds to 5′-CACCT sequences in candidate target genes. *J. Biol. Chem.* **274**, 20489–20498 (1999).
18. Conidi, A. *et al.* Few Smad proteins and many Smad-interacting proteins yield multiple functions and action modes in TGFβ/BMP signaling in vivo. *Cytokine Growth Factor Rev.* **22**, 287–300 (2011).
19. Comijn, J. *et al.* The two-handed E box binding zinc finger protein SIP1 downregulates E-cadherin and induces invasion. *Mol. Cell* **7**, 1267–1278 (2001).
20. Vandewalle, C. *et al.* SIP1/ZEB2 induces EMT by repressing genes of different epithelial cell-cell junctions. *Nucleic Acids Res.* **33**, 6566–6578 (2005).
21. Dai, Y.-H. *et al.* ZEB2 promotes the metastasis of gastric cancer and modulates epithelial mesenchymal transition of gastric cancer cells. *Dig. Dis. Sci.* **57**, 1253–1260 (2012).
22. Seuntjens, E. *et al.* Sip1 regulates sequential fate decisions by feedback signaling from postmitotic neurons to progenitors. *Nat. Neurosci.* **12**, 1373–1380 (2009).
23. Weng, Q. *et al.* Dual-mode modulation of Smad signaling by Smad-interacting protein Sip1 is required for myelination in the central nervous system. *Neuron* **73**, 713–728 (2012).
24. Van de Putte, T., Francis, A., Nelles, L., van Grunsven, L.A. & Huylebroeck, D. Neural crest-specific removal of Zfhx1b in mouse leads to a wide range of neurocristopathies reminiscent of Mowat-Wilson syndrome. *Hum. Mol. Genet.* **16**, 1423–1436 (2007).
25. Mowat, D.R. *et al.* Hirschsprung disease, microcephaly, mental retardation, and characteristic facial features: delineation of a new syndrome and identification of a locus at chromosome 2q22-q23. *J. Med. Genet.* **35**, 617–623 (1998).
26. Stanchina, L., Van de Putte, T., Goossens, M., Huylebroeck, D. & Bondurand, N. Genetic interaction between Sox10 an Zfhx1b during enteric nervous sstem development. *Dev. Biol.* **341**, 416–428 (2010).
27. Higashi, Y. *et al.* Generation of the floxed allele of the SIP1 (Smad-interacting protein 1) gene for Cre-mediated conditional knockout in the mouse. *Genesis* **32**, 82–84 (2002).
28. Jaegle, M. *et al.* The POU proteins Brn-2 and Oct-6 share important functions in Schwann cell development. *Genes Dev.* **17**, 1380–1391 (2003).
29. Jessen, K.R. & Mirsky, R. The origin and development of glial cells in peripheral nerves. *Nat. Rev. Neurosci.* **6**, 671–682 (2005).
30. Colognato, H. & Tzvetanova, I.D. Glia unglued: how signals from the extracellular matrix regulate the development of myelinating glia. *Dev. Neurobiol.* **71**, 924–955 (2011).
31. Brennan, A. *et al.* Endothelins control the timing of Schwann cell generation in vitro and in vivo. *Dev. Biol.* **227**, 545–557 (2000).
32. Druckenbrod, N.R., Powers, P.A., Bartley, C.R., Walker, J.W. & Epstein, M. L. Targeting of endothelin receptor-B to the neural crest. *Genesis* **46**, 396–400 (2008).
33. Xin, M. *et al.* Essential roles of the bHLH transcription factor Hrt2 in repression of atrial gene expression and maintenance of postnatal cardiac function. *Proc. Natl. Acad. Sci. USA* **104**, 7975–7980 (2007).
34. Leone, D.P. *et al.* Tamoxifen-inducible glia-specific Cre mice for somatic mutagenesis in oligodendrocytes and Schwann cells. *Mol. Cell. Neurosci.* **22**, 430–440 (2003).
35. Madisen, L. *et al.* A robust and high-throughput Cre reporting and characterization system for the whole mouse brain. *Nat. Neurosci.* **13**, 133–140 (2010).
36. Wu, L.M.N. *et al.* Zeb2 recruits HDAC-NuRD to inhibit Notch and controls Schwann cell differentiation and remyelination. *Nat. Neurosci.* http://dx.doi.org/10.1038/nn.4322 (2016).
37. Weider, M. *et al.* Chromatin-remodeling factor Brg1 is required for Schwann cell differentiation and myelination. *Dev. Cell* **23**, 193–201 (2012).
38. Bermingham, J.R. Jr. *et al.* Tst-1/Oct-6/SCIP regulates a unique step in peripheral myelination and is required for normal respiration. *Genes Dev.* **10**, 1751–1762 (1996).
39. Jaegle, M. *et al.* The POU factor Oct-6 and Schwann cell differentiation. *Science* **273**, 507–510 (1996).
40. Verstappen, G. *et al.* Atypical Mowat-Wilson patient confirms the importance of the novel association between ZFHX1B/SIP1 and NuRD corepressor complex. *Hum. Mol. Genet.* **17**, 1175–1183 (2008).
41. Berti, C. *et al.* Non-redundant function of dystroglycan and β1 integrins in radial sorting of axons. *Development* **138**, 4025–4037 (2011).
42. Yang, D. *et al.* Coordinate control of axon defasciculation and myelination by laminin-2 and -8. *J. Cell Biol.* **168**, 655–666 (2005).
43. Le, N. *et al.* Analysis of congenital hypomyelinating Egr2Lo/Lo nerves identifies Sox2 as an inhibitor of Schwann cell differentiation and myelination. *Proc. Natl. Acad. Sci. USA* **102**, 2596–2601 (2005).
44. Weber, D. *et al.* Mechanisms of epigenetic and cell-type specific regulation of Hey target genes in ES cells and cardiomyocytes. *J. Mol. Cell. Cardiol.* **79**, 79–88 (2015).
45. Woodhoo, A. *et al.* Notch controls embryonic Schwann cell differentiation, postnatal myelination and adult plasticity. *Nat. Neurosci.* **12**, 839–847 (2009).
46. Evans, E. *et al.* The behavioral phenotype of Mowat-Wilson syndrome. *Am. J. Med. Genet. A* **158A**, 358–366 (2012).
47. Pradier, B. *et al.* Smad-interacting protein 1 affects acute and tonic, but not chronic pain. *Eur. J. Pain* **18**, 249–257 (2014).
48. Emery, B. Regulation of oligodendrocyte differentiation and myelination. *Science* **330**, 779–782 (2010).
49. Li, H., He, Y., Richardson, W.D. & Casaccia, P. Two-tier transcriptional control of oligodendrocyte differentiation. *Curr. Opin. Neurobiol.* **19**, 479–485 (2009).
50. Arthur-Farraj, P.J. *et al.* c-Jun reprograms Schwann cells of injured nerves to generate a repair cell essential for regeneration. *Neuron* **75**, 633–647 (2012).
51. Adameyko, I. *et al.* Schwann cell precursors from nerve innervation are a cellular origin of melanocytes in skin. *Cell* **139**, 366–379 (2009).

ONLINE METHODS

Animals. All experiments involving mice were conducted according to the Lower Saxony State regulations for the use of experimental animals in Germany as approved by the Niedersächsisches Landesamt für Verbraucherschutz und Lebensmittelsicherheit (LAVES) and performed in compliance with the animal policies of the Max Planck Institute of Experimental Medicine. Mice were group-housed in individually vented cages with a 12 h light/dark cycle. Male and female mice were included in all experiments and randomly assigned to experimental groups according to age and genotype. *Zeb2*$^{loxP/loxP}$ mice[27] were bred to *Dhh-cre* transgenic mice[28]. *Dhh-cre*::*Zeb2*$^{loxP/loxP}$::*Ednrb*$^{loxP/loxP}$ mice were generated by breeding *Dhh-cre*::*Zeb2*$^{loxP/+}$::*Ednrb*$^{loxP/loxP}$ mice to *Zeb2*$^{loxP/loxP}$::*Ednrb*$^{loxP/loxP}$ mice[32]. Mice with a *loxP*-flanked *Hey2* (ref. 33) were acquired from Jackson Laboratories. *Dhh-cre*::*Zeb2*$^{loxP/loxP}$::*Hey2*$^{loxP/loxP}$ mice were generated by breeding *Dhh-cre*::*Zeb2*$^{loxP/+}$::*Hey2*$^{loxP/loxP}$ mice to *Zeb2*$^{loxP/loxP}$::*Hey2*$^{loxP/loxP}$ mice. Double *loxP*-flanked *Zeb2* littermates were used as experimental controls in all experiments unless indicated otherwise. *Plp1-creERT2*::*Zeb2*$^{loxP/loxP}$ mice were generated by breeding *Zeb2*$^{loxP/loxP}$ mice to *Plp1-creERT2* mice[34]. *loxP*-flanked *Zeb2* mice, *loxP*-flanked *Hey2* mice, *Plp1-creERT2* mice and *Dhh-cre* mice were on C57/Black6N background, while *loxP*-flanked *Ednrb* mice were on mixed C57Bl/6-SV129 background. Genotyping was performed on DNA isolated from tail or ear biopsies according to routine PCR methods using the following primers:

Dhh-cre sense 5′-CCTGCGGAGATGCCCAATTG-3′,
antisense 5′-CAGCCCGGACCGACGATGAA-3′;
Zeb2 loxP-flanked sense 5′-TGGACAGGAACTTGCATATGCT-3′,
anti-sense 5′-GTGGACTCTACATTCTAGATGC-3′;
Hey2 loxP-flanked sense 5′-CTAGAGAGGACCTGGAGAGTTTAAG-3′,
antisense 5′-CTGTGCCACCAGCCTTAAAACC-3′;
Ednrb wild-type allele sense 5′-CTGAGGAGAGCCTGATTGTGCCAC-3′,
antisense 5′-CGACTCCAAGAAGCAACAGCTCG-3′;
Ednrb loxP-flanked allele sense 5′-TGGAATGTGTGCGAGGCC-3′,
antisense 5′-CAGCCAGAACCACAGAGACCACCC-3′;
Plp1-creERT2 transgene sense 5′-TGGACAGCTGGGACAAAGTAAGC-3′,
antisense 5′-CGTTGCATCGACCGGTAATGCAGGC-3′.

Cell lines. The S16 cell line was directly obtained from producer Richard H. Quarles[52] at early passages. Identity of the cells was confirmed by PCR. The cell line was not tested for mycoplasma contamination.

Statistics. Whiskers in box–whisker blots show minima and maxima, and boxes extend from the first to the third quartiles with cross lines at the median. In dot plots, dots represent individual experiments or animals with cross lines at the mean ± s.d. or s.e.m. as indicated in the respective figure legends. When comparing two groups, statistics were performed using two-tailed Student's *t*-tests for unpaired samples assuming unequal variance. When comparing multiple groups, one-way ANOVA was performed except for experiments where $n = 3$, where Kruskal-Wallis one-way ANOVA was chosen. *P* values below 0.05 were considered significant (*P <0.05; **P <0.01; ***P <0.001). No statistical tests were used to predetermine sample sizes, but our sample sizes are similar to those generally employed in the field. Normal distribution of data was assumed, but not formally tested. All statistical analyses were performed using GraphPad Prism 6.00 or Microsoft Excel. A **Supplementary Methods Checklist** is available.

Induction of recombination, surgical procedures and footprint analysis. *Plp1-creERT2*::*Zeb2*$^{loxP/loxP}$ mice and *Zeb2*$^{loxP/loxP}$ mice were treated at the age of 6–8 weeks twice for 5 consecutive days with one daily intraperitoneal injection of 1 mg tamoxifen in corn oil with 10% analytical ethanol (all from Sigma) or the corn oil/ethanol mixture only (vehicle). Sciatic nerve crush or transection was performed under deep surgical anesthesia (ketamine hydrochloride 100 mg/kg and xylazine hydrochloride 5 mg/kg) at the sciatic notch. For crush injuries, the nerve was compressed for 15 s with fine forceps. To test early axon outgrowth ('pinch test'), mice were deeply anaesthetized 4 d after crush injury, the sciatic nerve was completely exposed and pinched with fine forceps starting from the distal end until a muscle reaction was observed. The observer was blinded regarding genotype and treatment of the mice and the regeneration distance (distance from the crush site to the pinch site where a reaction was observed) was measured with a ruler *in situ*. Footprints were acquired during the light phase by painting the hind feet of mice with black ink and letting them run along a 50-cm walking track. Prints were digitalized and the distance between toes 1 and 5 and the length of the print measured using the FOOTPRINTS program[53]. The sciatic functional index was calculated according to Inserra *et al.*[54]. The observer was blinded regarding the genotype of the mice.

Electrophysiological measurements. Electrophysiological measurements were performed under deep surgical anesthesia (ketamine hydrochloride 100 mg/kg and xylazine hydrochloride 5 mg/kg). Two recording electrodes were inserted into the intrinsic foot muscle, distal stimulation electrodes were inserted at the ankle and proximal stimulation electrodes were inserted at the sciatic notch. CMAPs were recorded with a Jaeger-Toennies Neuroscreen instrument. Nerve conduction velocities were calculated from the distance between proximal and distal stimulation electrodes (measured *in situ*) and the latency difference between the CMAPs after successive proximal and distal stimulation. CMAP amplitudes were calculated peak to peak.

Morphology and electron microscopy. For ultrastructural analysis, nerves were immersion fixed in 2.5% glutardialdehyde and 4% paraformaldehyde in phosphate buffer and embedded into epoxy resin (Serva). Semi-thin sections were cut at a thickness of 0.5 µm (Leica RM 2155 using a diamond knife Histo HI 4317, Diatome) and stained with a mixture of 1% toluidine blue and 1% azure II. Ultrathin sections were cut at a thickness of 50 nm, treated with uranyl acetate and lead citrate and analyzed with a Zeiss EM 900 (Leo). The G-ratio was defined as the numerical ratio between the fiber diameter and the diameter of the same fiber including its myelin sheath and measured on electron micrographs for at least 100 randomly chosen axons per animal and nerve ($n = 3$ animals per genotype and/or treatment group). Remyelinated fibers after sciatic nerve crush were counted on complete semi-thin cross-sections of sciatic nerves ($n = 3$ animals per genotype and/or treatment group). The percentage of myelinated and unmyelinated axons 56 d after nerve crush was quantified by counting all fibers on 25 randomly taken electron micrographs at 3,000× magnification per animal ($n = 3$ animals per genotype and treatment group). Axons per bundle were quantified on electron microscopic images by analyzing all axon–Schwann cell units where the nucleus of the Schwann cell was visible (amounting to 26 randomly chosen axon–Schwann cell units per animal and nerve on average, $n = 5$ animals per genotype). For G-ratio analysis, quantification of remyelinated fibers and quantification of axons per Schwann cell, the observer was blinded regarding the genotype and/or treatment (tamoxifen or vehicle) of the animals.

Immunohistochemistry. Samples were immersion fixed using 4% phosphate buffered paraformaldehyde and embedded into paraffin wax. Immunohistochemistry was performed on 5 µm thick sections using the heat-induced antigen retrieval method. Slides were boiled for 10 min in citrate buffer pH 6.0 with 0.05% Tween 20 (crushed nerves, **Fig. 1b**) or for 20 min in Tris/EDTA buffer pH 9.0 with 0.05% Tween 20 (**Fig. 1a**) and incubated with primary antibodies overnight at 4 °C. The following primary antibodies were used: Zeb2 (SC27-1984, Santa Cruz, 1:200), beta-III tubulin (TuJ1, MMS-435P, Covance, 1:250), Mbp (A0623, DAKO, 1:500), Krox20 (rabbit, 1:500)[55], Sox2 (SC1002, Millipore, 1:200), S100β (AB52642, Abcam, 1:500) and c-Jun (610327, BD Transduction). The following secondary antibodies were applied for 1 h at room temperature: Alexa Fluor® 555 donkey anti-mouse (A-31570), Alexa Fluor® 488 donkey anti-mouse (A-21202), Alexa Fluor® 555 donkey anti-rabbit (A-31572) and Alexa Fluor® 488 donkey anti-rabbit (A-21206) all from Molecular Probes, diluted 1:2,000. For each staining, samples from at least 3 individual animals per genotype (or treatment group) were processed simultaneously and used for the analysis. Sections were examined with a Zeiss Observer fluorescence microscope or Zeiss Axiophot brightfield microscope and images acquired with ZEN2 software (Carl Zeiss Microscopy). Images were processed with Adobe Photoshop 12.0.4, Adobe Illustrator CS5 and NIH Image J 1.46R.

RNA preparation, cDNA synthesis, real-time PCR and microarray analysis. RNA was isolated from sciatic nerves using the RNeasy Kit (Qiagen) according to manufacturer's instructions and the concentration and quality (ratio of absorption at 260/280 nm) evaluated using the NanoDrop spectrophotometer. Reverse transcription was performed with 1 µg of total RNA using the Superscript Kit (Invitrogen) and random nonamer primers. Quantitative real-time PCR was

performed in triplicates for each sample using SybrGreen (Life Technologies) and the ABI PRISM 7700 detection system (PerkinElmer). Four mice per genotype and/or treatment group were used in each experiment unless specified otherwise. Relative mRNA concentrations were determined using the threshold cycle method and normalized to *Rpl8*. Primer sequences can be found in **Supplementary Table 1**.

Luciferase reporter assay. Promoter regions for analysis of Zeb2 binding and repression were chosen using the Eukaryotic Promoter Database (http://epd.vital-it.ch/). The *Sox2* promoter region (chromosome 3 between positions 34,648,778 and 34,650,029, mouse genome version mm10) spanned positions –1,239 bp to +51 bp relative to the transcriptional start site of the *Sox2* gene, the *Hey2* promoter region (chromosome 10 between positions 30,842,764 and 30,845,280) positions –2,499 bp to +18 bp and the *Ednrb* promoter region (chromosome 14 between positions 103,844,229 and 103,846,824) positions –2,497 bp to +99 bp (variant Ednrb_1). Promoter regions were amplified by PCR and inserted as XhoI/XmaI fragments upstream of the luciferase gene into pGL2-luc (Promega). The following primers were used for PCR amplification: for *Sox2*, 5′-GCGCCCCGGGGGCAGGCAAGATTCTTGAAC-3′ and 5′-GCGCCTCGAGCTCTGCCTTGACAACTCCTG-3′; for *Hey2*, 5′-GCGCCCCGGGCTCTGACCCAGACGTAGGAC-3′ and 5′-GCGCCTCGAGCGGCTCCTGGAGGTTCTTTC-3′; and for *Ednrb*, 5′-GCGCCCCGGGGGTAGTTTAATGCGCCCATC-3′ and 5′-GCGCCTCGAGGCTGCTCCTAAACAGGCCTC-3′.

The S16 Schwann cell line was used for luciferase reporter gene assays. Cells were transfected using polyethylenimine on 3.5-cm tissue culture plates with 1.5 µg of luciferase reporter (pGL2-luc) and varying amounts (0.3 µg, 0.9 µg or 1.5 µg) of pCMV5-Zeb2expression vector. Cells were harvested 48 h post-transfection and luciferase activity was determined in the presence of luciferin substrate by detection of chemiluminescence.

BrdU injections and immunohistochemistry. BrdU was solubilized in water at a concentration of 10 mg/ml. Mice at the age of 10 or 25 d were injected intraperitoneally with one pulse of 100 µg/g body weight and killed 4 h later. Pregnant female mice at E18.5 were treated the same way and killed 70 min after the pulse. Sciatic nerves were embedded into wax and cut at a thickness of 5 µm. For detection of BrdU-positive nuclei, sections were boiled for 10 min at 100 W in a microwave in citrate buffer pH 6 and incubated for 30 min at room temperature in 0.2 M glycine followed by two washes in 100 mM disodium tetraborate pH 8.5. Anti-BrdU antibody (MAB3424, Millipore) was diluted 1:200 in 2% goat serum in PBS and applied overnight at 4 °C. After washing, the secondary antibody (Alexa555-anti-mouse, 1:2,000, A-31570, Molecular Probes) and DAPI (0.05 µg/ml) were applied for 1 h at room temperature. For quantification of proliferating cells, all BrdU/DAPI-positive nuclei were counted on cross-sections of sciatic nerves and values expressed as percentage of BrdU-positive cells relative to all DAPI-positive nuclei.

Chromatin immunoprecipitation (ChIP) assays. Pooled sciatic nerves from 15 P1 animals were dissected and immediately fixed in 1% PFA for 20 min at RT. Samples were washed once in phosphate-buffered saline, homogenized in 150 mM NaCl, 10% glycerol (vol/vol), 0.3% Triton X-100 (vol/vol) and 50 mM Tris-HCl (pH 8.0) containing protease inhibitor cocktail (Roche). Lysates were then sonicated with a Bioruptor sonicator (Diagenode) to approximately 500 bp. Sheared chromatin was incubated with 5 µg of Zeb2 antibody (SC27-1984, Santa Cruz) at 4 °C. ChIP was performed using the Magna ChIP G Kit (Merck Millipore) according to manufacturer's instructions. Quantitative real-time PCR was performed using SybrGreen (Life Technologies) and the ABI PRISM 7700 detection system (PerkinElmer). The relative fold enrichments were determined by the $2^{-\Delta CT}$ method and samples were normalized to input chromatin. Primers used for PCR analysis are provided in **Supplementary Table 1**.

Data availability. The primary data that support the findings of this study are available from the corresponding authors upon request.

52. Toda, K., Small, J.A., Goda, S. & Quarles, R.H. Biochemical and cellular properties of three immortalized Schwann cell lines expressing different levels of the myelin-associated glycoprotein. *J. Neurochem.* **63**, 1646–1657 (1994).
53. Klapdor, K., Dulfer, B.G., Hammann, A. & Van der Staay, F.J. A low-cost method to analyse footprint patterns. *J. Neurosci. Methods* **75**, 49–54 (1997).
54. Inserra, M.M., Bloch, D.A. & Terris, D.J. Functional indices for sciatic, peroneal, and posterior tibial nerve lesions in the mouse. *Microsurgery* **18**, 119–124 (1998).
55. Darbas, A. *et al*. Cell autonomy of the mouse claw paw mutation. *Dev. Biol.* **272**, 470–482 (2004).

doi:10.1038/nn.4321